Fractal dimensions of dynamically triangulated random surfaces

Christian Münkel, Dieter Heermann

Classification
Physics Abstracts
05.90 — 64.60A — 64.60F — 68.10 — 87.20C — 12.90

Short Communication

Fractal dimensions of dynamically triangulated random surfaces

Christian Münkel and Dieter W. Heermann

Institut für theoretische Physik, Philosophenweg 19, Universität Heidelberg,
D-6900 Heidelberg, Germany
and
Interdisziplinäres Zentrum für wissenschaftliches Rechnen der Universität Heidelberg, Germany

(Received 8 September 1992, accepted 16 September 1992)

Abstract. — Geometric properties of dynamically triangulated random surfaces in three-dimensional space can be described by fractal dimensions: the Hausdorff-dimension with respect to the embedding of the surfaces, the spectral and the spreading dimension for the intrinsic geometry. A remarkable dependence of the fractal dimensions on the bending rigidity is observed, even on the intrinsic dimensions.

1. Introduction.

The questions which we want to address in this paper are directed towards understanding the statistical mechanics of surfaces. We will consider random surfaces as two-dimensional manifolds with spherical topology embedded into three-dimensional Euclidian space. Specifically we are here interested in the conformational properties. Observables, which describe a conformation and are related to the two-dimensional manifold only, will be called intrinsic, those also related to the embedding extrinsic. All intrinsic observables define the intrinsic geometry of the surface (two-dimensional manifold). In the same way, the extrinsic geometry is described by extrinsic observables related to the three-dimensional embedding. The extrinsic geometry of a surface of given area, embedded in three-dimensional Euclidean space, depends on the bending rigidity. Excluded volume effects will not be taken into account. At high bending rigidity the surface will tend to be flat. As an example for an extrinsic property, the radius of gyration R_{gyr} of a surface with area A is then characterized by a law

$$R_{\mathrm{gyr}} \propto A^{1/d_{\mathrm{H}}} \qquad d_{\mathrm{H}} = 2 + \epsilon \tag{1}$$

where possibly the surface is still rough with an effective Hausdorff dimension d_{H} higher than 2 but $\epsilon > 0$ small.

At low bending rigidity we expect a convoluted surface and it is not *a priori* clear what the Hausdorff dimension [1], i.e. the extrinsic geometry of the surface is.

The surface itself can be fluid-like (in plane diffusion) or have a fixed intrinsic geometry (no in plane diffusion). The fixed intrinsic geometry does not necessarily mean an intrinsic dimension of 2. The surface may well have a higher intrinsic dimension, as well as a lower dimension. Consider a percolation cluster [2] constructed on a simple square lattice transfered into three-dimensional Euclidean space. This percolation cluster has an intrinsic geometry characterized by the spectral dimension $\tilde{d}_s$ of about 4/3 [3-5] and the spreading dimension $d_s \approx 1.46$ [6].

For a fluid-like surface the intrinsic geometry can change with the bending rigidity. The bending rigidity is induced by an extrinsic curvature and we can ask whether the intrinsic geometry adjusts to the extrinsic geometry.

For the type of model surface which we want to consider there is the possibility of a phase transition at a particular bending rgidity and we may ask: What is the geometry below, at and above the transition?

2. The model.

Here the surface, embedded into three-dimensional Euclidean space, is a triangulated sphere. This sphere has N nodes, $N_1 = 3(N-2)$ links, and $N_2 = 2(N-2)$ triangles. To study the intrinsic geometry we make the surface fluid-like by a dynamic triangulation [7-9]. Consider a situation as depicted in figure 1. The link which connects the nodes 1 and 3 can be "flipped" to connect the nodes 2 and 4, enabling in plane diffusion of the nodes. Thus the surface can be regarded as a fluid surface. The number of neighbours of a given point on the discrete surface is not fixed and can change and adjust to the extrinsic curvature.

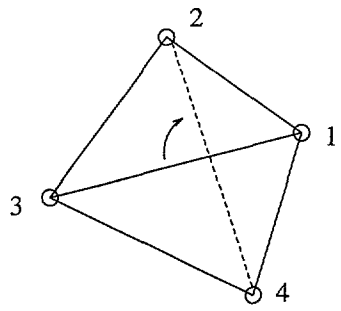

Fig.1. — Flip of a link in a triangulation

The statistical mechanics of the surface is specified as follows. The partition function is

$$\mathcal{Z}_N = \int \mathrm{d}^D X_0 \int \prod_{i=1}^{N-1} \mathrm{d}^D X_i \mathrm{e}^{-S} \tag{2}$$

Here, the translational mode is integrated out. The action or Hamiltonian (interaction energy) S is defined as

$$S = \underbrace{\beta \cdot \sum_{\langle i,j \rangle}^{N} (X_i^\mu - X_j^\mu)^2}_{S_g} + \underbrace{\lambda \cdot \sum_{\Delta_i, \Delta_j} (1 - \hat{\mathbf{n}}_{\Delta_i} \hat{\mathbf{n}}_{\Delta_j})}_{S_e} - \underbrace{\alpha \cdot \sum_{i=0}^{N} \log q_i}_{S_m} \tag{3}$$

The Gaussian action S_g is a sum over the positions X in embedding Euclidian space of all nearest neighbour nodes, i.e. all links of the triangulation. We shall use $\beta = 1$, because of the rescaling invariance of the action. A different value for β would rescale only the overall size of the whole surface or equivalently the length scale of the model. This term will give rise to an average area, which is proportional to the number of nodes N.

S_e is an edge extrinsic curvature term [10-17] $\sum_{\Delta_i,\Delta_j}$ denotes a summation over all adjacent triangles which share an edge (i,j). The product $\hat{\mathbf{n}}_{\Delta_i} \cdot \hat{\mathbf{n}}_{\Delta_j}$ is the scalar product of the vectors normal to the triangles with the common edge (i,j).

The third part of the action S is the measure action S_m. Let q_i denote the number of nearest neighbours of node i, then $\sigma_i = q_i/3$ is the volume of the dual image of node i and the discrete analog of the invariant volume $\int d^2\xi \sqrt{g}$ with metric g [7, 9, 18, 19] S_m is derived from the discretization $\prod_i dX_i \sigma_i^{D/2}$ of the invariant Fujikawa measure [20]. Therefore we used $\alpha = \dfrac{D}{2}$ throughout this work.

This model shows a peak (cusp) of the specific heat at $\lambda_c \approx 1.47$, which is interpreted as a phase transition [21-28]. Below λ_c the surface is collapsed while above the surface may be essentially flat. This is in sharp contrast to self-avoiding fluid surfaces, which cannot collaps, but are expected to form branched polymers at length scales larger than the persistence length [29].

We use the standard Monte Carlo algorithm [30-32] to calculate thermodynamic averages. One Monte Carlo sweep is completed when each triangulation point was given the chance for a displacement in the embedding space ($\Delta X_i^\mu \in [0; 0.2]$ at $\lambda = 3.0$, $\Delta X_i^\mu \in [0; 0.9]$ at $\lambda = 0.0$) from its previous position and the edges of the triangulation were given the chance to re-connect or flip to an orthogonal position.

For the simulations presented below we used the parallel transputer machine of the Interdisziplinäres Zentrum für wissenschaftliches Rechnen as well as a cluster of workstations. Because of the dynamic triangulation with link flips we could neither vectorize nor parallelize the program. Thus on each of the processors we run one set of data to obtain independent measurements. The performance was approximately 0.001 s per update of a node on a workstation. At $\lambda = 0$ the performance was about two times higher. One $T800$ Transputer was ten times slower than a workstation approximately.

We decided not to use the parallel link flip method [33, 22], because this method produces ϕ^3-graphs including tadpoles and self-energy parts. The dual meshes (i.e. triangulations) are different from the ones prepared with the single link flip method. In addition, the acceptance rate of link flips decreases down to 1% at the phase transition $\lambda \approx 1.5$ [22], which is much smaller than the value of about 30% for the single link flip method.

We simulated surfaces with up to 25596 triangles for the sphere. Up to one million Monte Carlo steps per node for each N and λ were necessary to obtain good averages. The simulations started with systems, which were equilibrated during several tenthousand steps per node, depending on the size and rigidity. These clearly exceeds earlier simulations, except simulations in space dimensions $D = 0, -2$. In those cases, the recursive sampling technique [33-35] enables

one to handle more than one million triangles. Unfortunately, this method is not applicable to positive space dimensions up to now.

2.1 EXTRINSIC FRACTAL DIMENSIONS. — To investigate the extrinsic geometry of the surface we imagine the nodes of the surface to form a cluster in the embedding space. We can then calculate the cluster fractal dimension [1] as the dimension characterizing the surface. The usual definition for the fractal dimension (which we take as the Hausdorff dimension d_H for random surfaces [19,36-39]

$$d_H = \lim_{N\to\infty} \left(\frac{2 \ln N}{\ln \langle R^2 \rangle} \right) \tag{4}$$

But there is an ambiguity in measuring the *linear size* R of a random surface. One can use the radius of gyration R_{gyr} as a measure

$$\langle R^2_{gyr} \rangle = \frac{1}{N(N-1)} \left\langle \sum_{i<j}^{N} (X_i - X_j)^2 \right\rangle \tag{5}$$

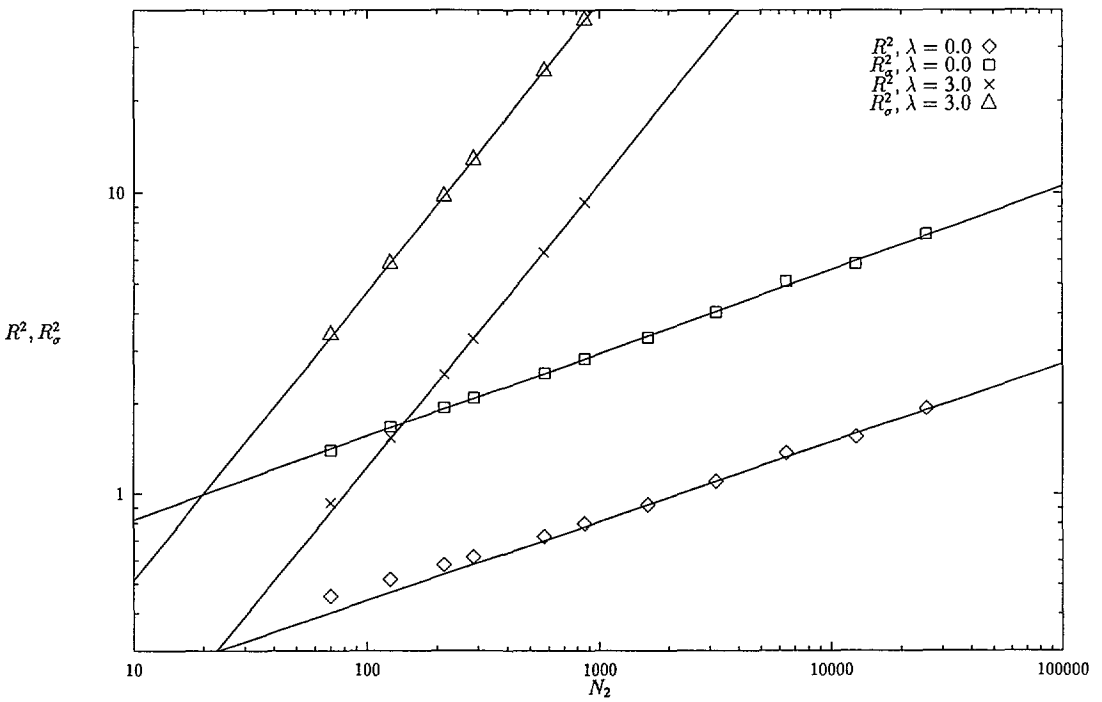

Fig.2. — Size dependence of the radius of gyration (Eqs. (5) and (6)) at the highest rigidity $\lambda = 3.0$ $[R^2(\times), R^2_\sigma(\triangle)]$ and zero rigidity $\lambda = 0.0$ $[R^2(\diamond), R^2_\sigma(\square)]$. Statistical errors are smaller than symbol sizes.

In this definition all nodes are treated as equal, regardless of the intrinsic geometry. We may take the intrinsic geometry into account and define the radius of gyration R_σ as a weighted cluster radius

$$\langle R_\sigma^2 \rangle = \frac{1}{N(N-1)} \left\langle \sum_{i<j}^{N} \sigma_i \sigma_j (X_i - X_j)^2 \right\rangle \quad , \tag{6}$$

with the intrinsic area element proportional to σ_i.

Another possible choice for the linear size is the box radius B

$$B = \sup \{ |X_i - X_j| : j = 1..\ N, i < j \} \tag{7}$$

The fractal dimension may be computed as the asymptotic slope of a log-log plot as in figure 2. Table I shows the results for the Hausdorff dimensions as a function of the extrinsic curvature λ for two of the possible choices of linear size. For the box radius we find that

$$\langle B^2 \rangle \propto \langle R_{\mathrm{gyr}}^2 \rangle \ln N \tag{8}$$

for all λ less than or equal λ_c, in agreement with the results for fixed triangulations at zero rigidity [40, 41].

Table I. — *Cluster fractal dimensions (Hausdorff-dimension)* d_H.

λ	0.0	0.50	1.0	1.47	1.75	3.0
$d_H[R_\sigma]$	7.2(3)	6.7(6)	5.8(4)	3.0(4)	2.09(2)	2.08(3)
$d_H[R]$	7.6(6)	7.7(7)	5.5(8)	3.0(4)	2.13(2)	2.12(3)

For $\lambda \geq \lambda_c$ all three definitions of the linear size of the random surface result in the same value d_H within errors. In the limit of infinite rigidity the surface is flat, $d_H(\lambda \to \infty) \to 2$.

A remarkable result is, that even at *zero rigidity* ($\lambda = 0$) d_H is still finite. This is in agreement with the prediction of a scaling phase for $D = 3, \lambda = 0$ and $\alpha = \frac{D}{2}$ [9]. Our model neglects excluded volume effects and thus allows for Hausdorff dimensions above 3. A finite Hausdorff dimension is in sharp contrast to models using Regge calculus [42] and to random surfaces with *fixed* connectivity. There one finds $d_H = \infty$ ($R_{\mathrm{gyr}}^2 \propto \log N$ [14, 40, 41, 43, 44]. *Dynamically* triangulated surfaces show an extraordinarily large but still finite fractal dimension below the phase transition. Our data exclude a logarithmic fit ($d_H = \infty$), which was prefered by Renken and Kogut [25] and Baillie *et al.* [27]. This can be explained by the fact, that they used triangulations with up to 288 (144) nodes only. At $\lambda = 0$ the asymptotic scaling regime starts there.

There may be a jump in d_H at the critical point $\lambda_c \approx 1.47$. For $\lambda > \lambda_c$ the surface is essentially flat. Of course, the surface may be rough, leading in our estimate of the Hausdorff dimension to a higher value than 2. At λ_c the value is higher than 2 and increases with decreasing bending rigidity. Considering the different discretization of the extrinsic curvature term, the result $d_H[R] = 2.1(1)$ at $\lambda = 1.5$ on ϕ^3-graphs [22] seems to confirm this prediction. Baillie *et al.* [27] predicted a change of d_H from 2 at large λ to 4 at the transition, but they used $\alpha = -1.5$ and smaller triangulations. In a later work [24], they excluded $d_H = 4$ at the phase transition after an analysis of simulations with $\alpha = -1.5, 0, 1.5$.

Using much smaller meshes and less Monte Carlo steps, Billoire and David [19] reported $d_H[R_\sigma] = 4.2(5)$ in $D = 12$ space dimensions at zero rigidity. This is comparable to the result $d_H[R_\sigma] = 4.9(1)$ in $D = 10$ of Jurkiewicz, Krzywicki and Petersson [45], who also measured $d_H[R_\sigma] = 8.3(1)$ in $D = 3$. This value may be to high, because the used triangulations with $N_2 = 100, 196$ for their analysis too, which are not in the asymptotic regime ($N_2 > 200, \lambda = 0$).

2.2 SPREADING DIMENSION d_s. — Contrary to regular and fixed triangulated random surfaces, the *intrinsic* dimension is not known *a priori*, not even at vanishing rigidity, but may be described by the spreading dimension d_s [6].

Within the context of percolation clusters, the spreading dimension is determined by the average number A_n of distinct sites that are accessible from a given origin along cluster bonds in at most n steps, n large: $A_n \propto n^{d_s}$ For a regular and fixed triangulation with coordination number $q = 6$ the number A_n of distinct nodes connected to a fixed node grows as

$$A_n = 6 + 12 + 18 + . \quad + 6n = 6 \sum_{x=1}^{n} x = 3\, n(n+1) \propto n^2 \tag{9}$$

and the spreading dimension is two. This may be verified also by the scaling of the length $l(n)$ of the boundary at distance n, which scales as $l(n) = 6n$, reproducing $d_H = 2$.

Because of the periodic boundary conditions resulting from the spherical topology of the dynamically triangulated surface, we used a slightly different definition [19] using the number N_2 of triangles

$$d_s = \lim_{N_2 \to \infty} \frac{\ln N_2}{\ln \langle d_{ij} \rangle} \tag{10}$$

using the mean geodesic distance

$$\langle d_{ij} \rangle = \left\langle \frac{1}{N^2} \sum_{i,j} d(i,j) \right\rangle . \tag{11}$$

The geodesic distance $d(i,j)$ between two nodes i and j describes the minimal number of links, connecting the two nodes.

In figure 3, the size dependence $\langle d_{ij} \rangle (N_2)$ is shown for the highest and zero rigidity. The results of runs with up to 25596 triangles and one million Monte Carlo steps per node for each N_2 and λ are summarized in table II.

Table II. — *Spreading dimension d_s of dynamically triangulated random surfaces at different bending rigidities.*

λ	0.00	0.50	1.00	1.47	1.75	3.00	regular
d_s	2.62(3)	2.61(4)	2.57(8)	2.29(2)	2.27(1)	2.24(1)	2.00

Because of the periodic boundary conditions and the term proportional to n in equation (9), even $\langle d_{ij}(N_2) \rangle$ for a regular triangulated torus approaches the ideal power law behaviour from below. Of course, the deviations of the effective exponents from the exact value are very small: $d_s[200\,.\,.\,512] = 1.988$ and $d_s[512\,.\,.\,1800] = 1.996$. The data underlying table II are well fitted by a pure power law, at least above $N_2 \approx 100$.

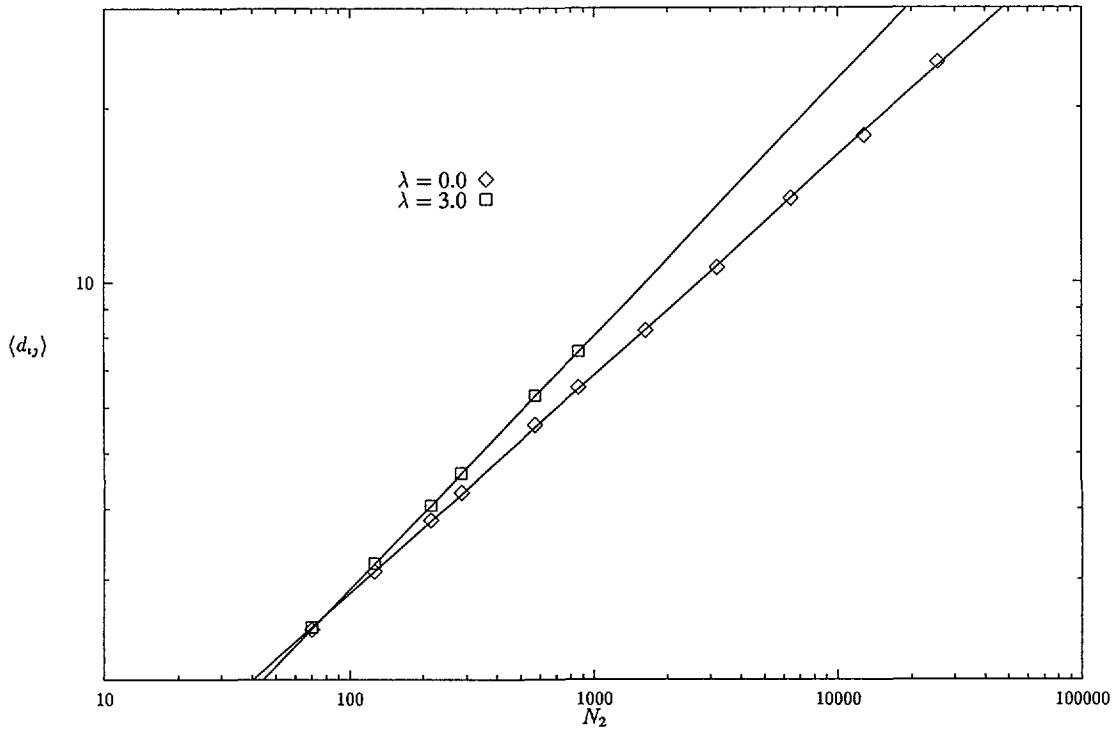

Fig.3. — Size dependence of the mean geodesic distance (11) at the highest rigidity $\lambda = 3.0$ (□) and vanishing rigidity $\lambda = 0.0$ (◇). Statistical errors are smaller than symbol sizes.

It is surprising, that the strength of the bending rigidity introduced by the extrinsic curvature term influences the intrinsic geometry also: the surface becomes more flat. Although an extrapolation $\lambda \rightarrow \infty$ to infinite bending rigidity suggests a flat surface with respect to the embedding, $d_H(\lambda \rightarrow \infty) = 2$, it does not suggest a intrinsic flat surface: $d_s(\lambda \rightarrow \infty) > 2.2$. This λ-dependence of d_s has important consequences. For instance, within the framework of finite size scaling the correlation length ξ is compared to the linear size L of the system. Usually scaling was done with N_2, but the intrinsic size of a random surface is related to the intrinsic area N_2 by $L \approx N^{1/d_s}$ and therefore depends on λ.

It is interesting to compare these results in three-dimensional space with those in $D = 12$. At zero rigidity, Billoire and David [19] reported $d_s = 2.0(2)$. This value changes to $d_s = 3.2(2)$, if α equals zero. If an Ising model is coupled to ϕ^3 graphs, i.e. dynamically triangulated random surfaces in $D = 0$, one obtains $d_s = 2.78(4)$ [46] Coupling to $C = -2$ matter results in $d_s \approx 2.5$ or $d_s \approx 3.5$ [35], according to the measurement of the number and the total length of boundaries at the distance r or the number of triangles within the distance r respectively. Suprisingly, for simulations in $D = 0$ with the parallel flip and the recursive sampling technique no scaling behaviour was found because of an anomalous increase of the number of branches [33, 34, 47].

2.3 SPECTRAL-DIMENSION $\tilde{d}_s$. — The different properties of fractals may not be described by the spreading dimension d_s alone. Another important intrinsic property is the spectral dimension, which may be definded by the exponent d_w, describing the long time behaviour

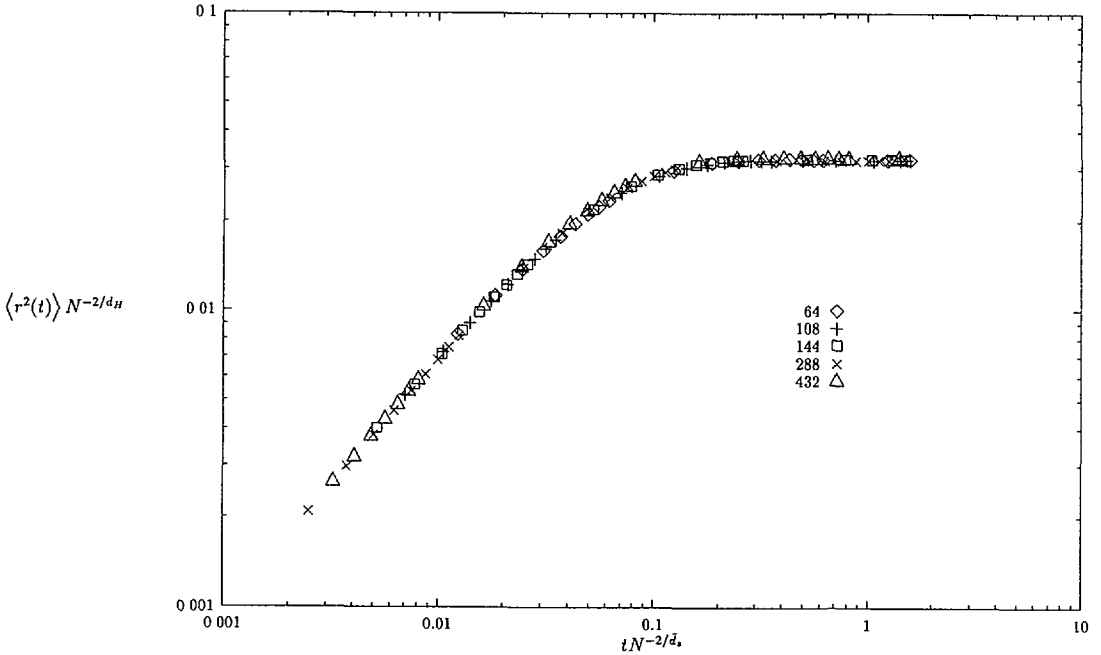

Fig.4. — Scaling plot (Eq. (14)) for the spectral dimension $\tilde{d}_s$ at the highest rigidity $\lambda = 3.0$.

$t \to \infty$ of the mean end-to-end distance $\langle r^2\rangle(t)$ of a random walk with t steps on the triangulation:

$$\langle r^2\rangle(t) \propto t^{2/d_w} \ , \ (t \to \infty). \tag{12}$$

Computing the spectral dimension $\tilde{d}_s$ also requires the Hausdorff-dimension d_H of the surface [4, 5]

$$\tilde{d}_s = \frac{2\, d_H}{d_w} \tag{13}$$

In general, this quantity may differ from the spreading dimension, for example for percolation-clusters [6].

Starting with $\langle r^2(t)\rangle \propto t^{\tilde{d}_s/d_H}$, one can describe $\langle r^2(t)\rangle$ with the crossover scaling form [48]

$$\langle r^2(t)\rangle = N^{2/d_H} \ \mathcal{F}\left(t\, N^{-2/d_s}\right). \tag{14}$$

One has $\mathcal{F}(x) \propto x^{\tilde{d}_s/d_H}$ for $x \ll 1$ and because of the periodic boundary conditions of the spherical topology for $x \gg 1$ $\mathcal{F}(x) = \text{const}$. The crossover time $\tau = N^{2/\tilde{d}_s}$ is nearly reached, if the random walk length equals the number of nodes of the surface. In a scaling plot following equation (14) the Hausdorff-dimension d_H and the spectral dimension are determined by collapsing all the data onto one master curve. Figure 4 shows this for the highest rigidity $\lambda = 3.0$.

Table III. — *Spectral dimensions $\tilde{d}_s$ of the sphere.*

λ	0.00	0.50	1.00	1.47	1.75	3.00	regular
$\tilde{d}_s$	1.75(10)	1.8(1)	1.8(2)	1.85(15)	1.83(5)	1.90(5)	2.00

The results of the scaling plots are tabulated in table III.

These results should be compared with those of dynamically triangulated self-avoiding vesicles $\tilde{d}_s = 2.02(4)$ [48].

Acknowledgements.

Partial support by the SFB 123 and the BMFT project 0326657D and 031240284 is gratefully acknowledged.

References

[1] Feder J., Fractals (Plenum Press, 1988).

[2] Stauffer D. and Aharony A., Introduction to Percolation Theory, 2nd ed. (Taylor and Francis, 1992).

[3] H. E. Stanley Ed., On Growth and Form; Fractal and Non-Fractal Patterns in Physics (Nijhoff, 1986).

[4] Rammal R. and Toulouse G., *J. Phys. Lett. France* **44** (1983) L13.

[5] Alexander S. and Orbach R., *J. Phys. France* **43** (1982) L625.

[6] Vannimenus J., Nadal J. and Martin H., *J. Phys. France* **17A** (1984) L351.

[7] Ambjørn J., Durhuus B. and Fröhlich J., *Nucl. Phys.* **B257** (1985) 433.

[8] David F., *Nucl. Phys.* **B257** (1985) 543.

[9] Boulatov D., Kazakov V., Kostov I. and Migdal A., *Nucl. Phys.* **B275** (1986) 641.

[10] Peliti L. and Leibler S., *Phys. Rev. Lett.* **54** (1985) 1690.

[11] Helfrich W., *J. Phys. France* **46** (1985) 1263.

[12] Förster D., *Phys. Lett.* **114A** (1986) 115.

[13] Polyakov A., *Nucl. Phys.* **268B** (1986) 406.

[14] Ambjørn J. and Durhuus B., *Phys. Lett.* **B188** (1987) 253.

[15] Ambjørn J., Durhuus B. and Jonsson T., *Phys. Rev. Lett.* **58** (1987) 2619.

[16] Ambjørn J., Durhuus B., Fröhlich J. and Jonsson T., *Nucl. Phys.* **B290** (1987) 480.

[17] Espriu D., *Phys. Lett.* **194B** (1987) 271.

[18] Ambjørn J., Durhuus B. and Jonsson T., *Nucl. Phys.* **B275** (1986) 161.

[19] Billoire A. and David F., *Nucl. Phys.* **B275** (1986) 617.

[20] Fujikawa K., *Nucl. Phys.* **B226** (1985) 437.

[21] Münkel C. and Heermann D., to be published (1992).

[22] Catteral S., Eisenstein D., Kogut J. and Renken R., *Nucl. Phys.* **B366** (1991) 647.

[23] Renken R. and Kogut R., *Nucl. Phys.* **B354** (1991) 328.

[24] Baillie C., Williams R., Catteral S. and Johnston D., *Nucl. Phys.* **B348** (1991) 543.

[25] Renken R. and Kogut R., *Nucl. Phys.* **B348** (1991) 580.

[26] Catteral S., *Phys. Lett.* **B243** (1990) 121.

[27] Baillie C., Johnston D. and Williams R., *Nucl. Phys.* **B335** (1990) 469.

[28] Catteral S., *Phys. Lett.* **B220** (1989) 207.

[29] Kroll D. and Gompper G., *Science* **255** (1992) 968.

[30] Kalos M. and Whitlock P., Monte Carlo Methods, volume 1 (Wiley, New York, 1986).

[31] Heermann D., Computer Simulation Methods in Theoretical Physics, 2nd ed. (Springer Verlag, Heidelberg, 1990).

[32] Binder K. and Heermann D., Monte Carlo Simulation in Statistical Physics (Springer-Verlag Heidelberg, 1988).

[33] Agishtein M. and Migdal A., *Nucl. Phys.* **B350** (1991) 690.

[34] Agishtein M., Benav R., Migdal A. and Solomon S., *Mod. Phys. Lett.* **A6** (1991) 1115.

[35] Kawamoto N., Kazakov V., Saeki Y. and Watabiki Y., *Nucl. Phys. B (Proc. Suppl.)* **26** (1992) 584.

[36] Ambjørn J., Durhuus B. and Jonsson T., *Nucl. Phys.* **B316** (1989) 526.

[37] Harnish R. and Wheater J., *Nucl. Phys.* **B350** (1991) 861.

[38] Renken R. and Kogut J., *Nucl. Phys.* **B342** (1990) 753.

[39] Baig M., Espriu D. and Wheater J., *Nucl. Phys.* **B314** (1989) 587.

[40] Heermann D., *Int. J. Mod. Phys.* **C2** (1991) 613.

[41] Billoire A., Gross D. and Marinari E., *Phys. Lett.* **139B** (1984) 75.

[42] Gross M. and Hamber H., *Nucl.Phys.* **B354** (1991) 703.

[43] Duplantier B., *Phys. Lett.* **141B** (1984) 239.

[44] Gross D., *Phys. Lett.* **138B** (1984) 185.

[45] Jurkiewicz J., Krzywicki A. and Petersson B., *Phys. Lett.* **168B** (1986) 273.

[46] Baillie C., *Nucl. Phys. B (Proc.Suppl.)* **26** (1992) 566.

[47] Agishtein M., Jacobs L., Migdal A. and Richardson J., *Mod. Phys. Lett. A* **5** (1990) 965.

[48] Komura S. and Baumgärtner A., *J. Phys. France* **51** (1990) 2395.